



## Annulight Workshop 4

Low-order modelling of the  
nonlinear response of turbulent flames

**Nicolas Noiray**

[noirayn@ethz.ch](mailto:noirayn@ethz.ch)

# Contents

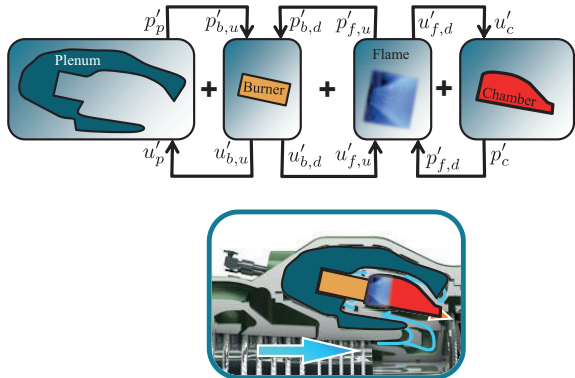
1 Thermoacoustic networks

2 Low order modelling

3 Limit cycle amplitude dynamics

4 Super- and subcritical Hopf bifurcation

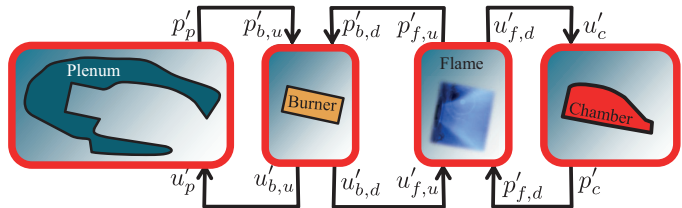
# Reduced order modeling with thermoacoustic networks



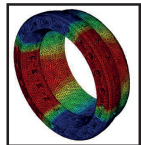
- One alternative approach to LES is to simulate only the acoustics (potential flow) and drop the simulations of the fluid mechanics
- To do so, we decompose the acoustic network into several elements (plenum, burner flame, chamber). All these elements are described "acoustically"
- The effect of the fluid mechanics (NS equations) are incorporated into the transfer matrices which relate the different elements
- This modelling strategy can be used for predictions of the thermoacoustic instabilities

Thermoacoustic networks are an efficient way to model the instabilities. The complexity is reduced by splitting the system into sub-components. Their dynamics must be modeled separately

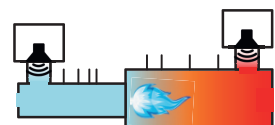
# Thermoacoustic networks



Plenum and chamber:  
Input-output relationship from  
analytic model or FEM

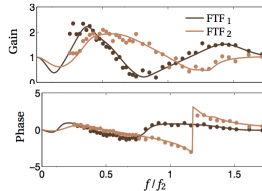


Burner and flame:  
Single burner experiments  
or CFD



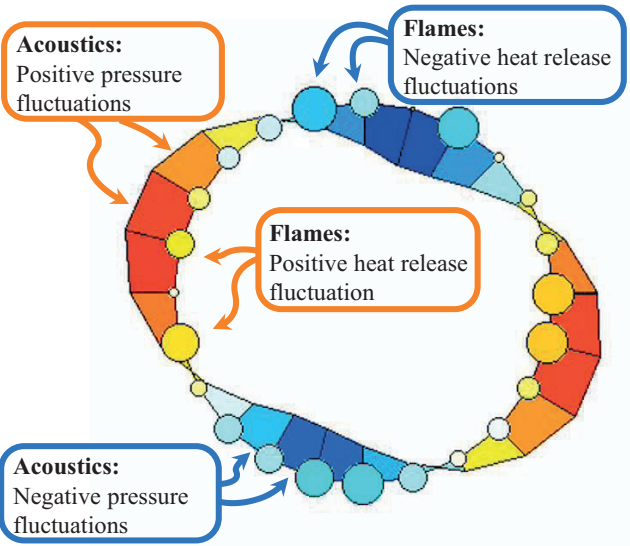
Noiray et al., Combustion  
Theory and Modeling 2011

$$\begin{pmatrix} p'_{f,u} \\ u'_{f,d} \end{pmatrix} = \begin{pmatrix} T_{11} & T_{12} \\ T_{21} & T_{22} \end{pmatrix} \begin{pmatrix} p'_{f,d} \\ u'_{f,u} \end{pmatrix}$$



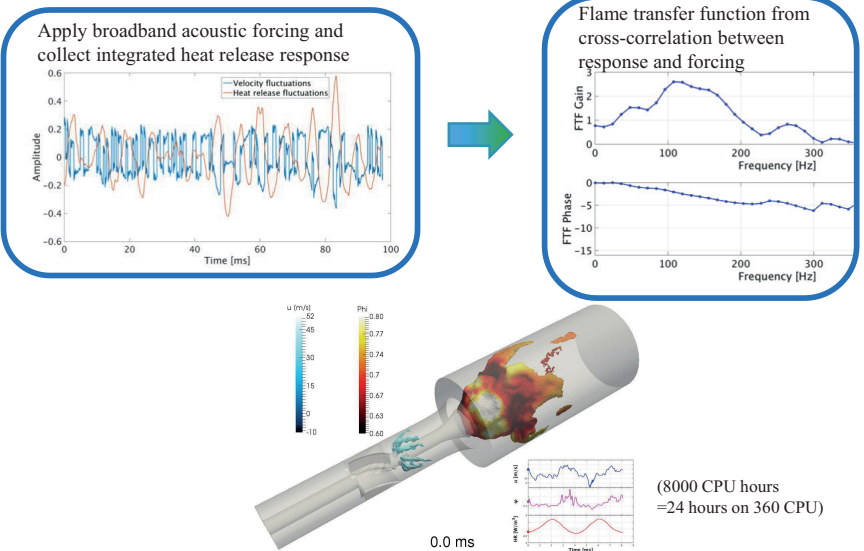
- For the acoustic propagation inside the combustion chamber and the plenum, you can use analytic expressions or FEM to solve the Helmholtz equation inside the domain, which exhibits temperature gradients
- For the burner and the flame, we can do measurements of the transfer matrices which are obtained by forcing the flame with loudspeakers upstream and downstream of the chamber, recording with microphones the incident and reflected ac. wave of both sides of the flame. With this, we can compute the reflection and transmission coefficients for downstream and upstream excitations. From this, the scattering matrix is obtained from which we can compute the transfer matrix
- One important element of the transfer matrix is the transfer function which relates the acoustic velocity jump across the flame
- The output from the flame is a product of the complex combustion process occurring at the burner outlet, which leads to a nontrivial flame transfer function (FTF)
- Small variation of operating condition can lead to a huge variation of the flame transfer function and hence has a significant influence on the thermoacoustic stability of the system

# Thermoacoustic networks



- With such a thermoacoustic network, we can simulate the thermoacoustic instability in an annular chamber, as we see to the left
- Circles correspond to flames, colored by their heat release rate fluctuations (more red for positive, more blue for negative)
- Bars correspond to acoustic pressure fluctuations, same coloring as flames
- Model incorporates FEM simulations of chamber and measured FTFs
- We observe an annular spinning mode where the heat release rate and the acoustic pressure fluctuations are in phase
- With such a tool, we can develop different burner variants and plug them into the network to do predictions of the acoustic instabilities, which saves a lot of testing and labor costs
- This will be a topic in the lecture 2 weeks from now
- Simulation from Noiray, Bothien and Schuermans (Combustion Theory and Modelling 2011)

# Prediction of FTF from simulations



- Challenge now is to develop system identification tools to extract in a computationally efficient way the Nonlinear MIMO response
- Alternatively, we can do numerical simulations to get the FTF
- There are also challenges here, especially that we have to rely on the quality of the simulation, but it is possible
- From a research perspective, it is generally good to do experiments and simulations of this multidisciplinary problem to better understand the coupling

# Contents

1 Thermoacoustic networks

2 Low order modelling

3 Limit cycle amplitude dynamics

4 Super- and subcritical Hopf bifurcation

# Galerkin expansion (1/4)

We now consider the case of sound field generated by sources in enclosures.

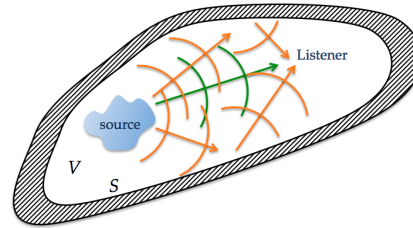
We limit ourselves to the case of rigid walls cavities  $\Rightarrow \mathbf{u}' = 0 \equiv \nabla_{\perp} p' = 0$

$\equiv Z = p'/u' \rightarrow \infty$ . We take again the K-H integral equation to express the acoustic pressure.

We have to find the adequate Green's function which satisfies the physical boundary condition and allows us to use the expression:

$$P(\mathbf{x}) = \int_V G(\mathbf{x}|y) S(y) dV \quad (1)$$

The natural eigenmodes of the cavity  $\psi_j$  are solution of the *homogeneous* Helmholtz equation and they constitute



an orthonormal basis. It is therefore reasonable to express the appropriate Green's function as a sum of these eigenmodes. This powerful method is called a Galerkin expansion:

$$G(\mathbf{x}|y) = \sum_{j=1}^{\infty} A_j \psi_j(\mathbf{x}) \quad (2)$$

- The field satisfies the Helmholtz equation with rigid boundary condition

$$\nabla^2 P(\mathbf{x}) + k^2 P(\mathbf{x}) = S(\mathbf{x}) \quad \text{in } V \quad (3)$$

$$\text{and } \nabla_{\perp} P = 0 \quad \text{on } S \quad (4)$$

We consider a Green function solution of

$$\nabla^2 G(\mathbf{x}|y) + k^2 G(\mathbf{x}|y) = \delta(\mathbf{x} - \mathbf{y}) \quad \text{in } V \quad (5)$$

$$\text{and } \nabla_{\perp} G(\mathbf{x}|y) = 0 \quad \text{on } S \quad (6)$$

We can then deduce the K-H integral equation by multiplying the inhomogeneous Helmholtz equation for  $P$  by  $G$ , the one for  $G$  by  $P$ , subtracting them, integrating over the volume and making use of the Gauss theorem. Using a Green's function satisfying the physical boundary condition, the surface integral vanishes:

$$\int_S [P(y) \nabla G(x|y) - G(x|y) \nabla P(y)] dS = P(x) - \int_V G(x|y) S(y) dV$$

## Galerkin expansion (2/4)

### Projection basis $\psi$ used to expand the Green's function

The eigenmodes  $\psi_j$  are solutions of the homogeneous Helmholtz equation at specific frequencies  $\omega_j$ , which are the cavity eigenfrequencies:

$$\nabla^2 \psi_j + \left(\frac{\omega_j}{c}\right)^2 \psi_j = 0 \quad \text{in } V$$

and  $\nabla_{\perp} \psi_j = 0 \quad \text{on } S$

As already mentioned they form an orthonormal basis with

$$\int_V \psi_n \psi_m^* dV = V \Lambda_n \delta_{nm}$$

and  $\Lambda_n = \frac{1}{V} \int_V |\psi_n|^2 dV$  is the mode normalisation factor.

For rigid walls,  $\psi_i$  are real functions. The more general case of boundaries with distributed *finite* impedance at the walls can also be treated using the eigenfunctions solution of the homogeneous Helmholtz equation and satisfying the physical boundary conditions. However, the eigenfunctions are in that case imaginary and depend on the frequency. One can for example find this more complex derivation in the classical *Morse & Ingard (1968) Theoretical Acoustics*.

We now look for the coefficients  $A_j$  in (2) to have an explicit formulation of our Green's function. If we substitute (2) into (5), multiply by  $\psi_m$  and integrate over the volume  $V$ , one get

$$\int_V \psi_m(x) \nabla^2 \sum_{j=1}^{\infty} A_j \psi_j(x) + k^2 \psi_m(x) \sum_{j=1}^{\infty} A_j \psi_j(x) dV = \int_V \delta(x - y) \psi_m(x) dV$$

$$\text{which gives } \int_V \sum_{j=1}^{\infty} [\psi_m(x) \nabla^2 (A_j \psi_j(x)) + k^2 \psi_m(x) A_j \psi_j(x)] dV = \psi_m(y)$$

Considering that by definition,  $\nabla^2 (A_j \psi_j(x)) = -A_j k_j^2 \psi_j(x)$ , with  $k_j = \omega_j/c$ , one can write

$$\sum_{j=1}^{\infty} (k^2 - k_j^2) A_j \int_V \psi_m(x) \psi_j(x) dV = \psi_m(y)$$

Thanks to the orthogonality of the projection basis, we can deduce that

$$A_m (k^2 - k_m^2) V \Lambda_m = \psi_m(y) \quad \text{and therefore} \quad A_m = \frac{\psi_m(y)}{V \Lambda_m (k^2 - k_m^2)}$$

## Galerkin expansion (3/4)

The Green function satisfying the physical boundary conditions has been identified and expressed as

$$G(\mathbf{x}|\mathbf{y}) = \sum_{j=1}^{\infty} A_j \psi_j(\mathbf{x}) = \sum_{j=1}^{\infty} \frac{\psi_j(\mathbf{y})\psi_j(\mathbf{x})}{V\Lambda_j(k^2 - k_j^2)}$$

### Acoustic field in the rigid wall cavity or room

From equation (1), the acoustic field  $p'(\mathbf{x}, t) = P(\mathbf{x}, \omega)e^{i\omega t}$  inside the rigid-wall cavity produced by the harmonic distributed source  $\mathcal{S}(\mathbf{y}, t) = S_\omega(\mathbf{y})e^{i\omega t}$  is

$$P(\mathbf{x}, \omega) = \sum_{j=1}^{\infty} \hat{\eta}_j(\omega) \psi_j(\mathbf{x}) \quad \text{with} \quad \hat{\eta}_j(\omega) = \frac{c^2}{V\Lambda_j(\omega^2 - \omega_j^2)} \int_V \psi_j(\mathbf{y}) S_\omega(\mathbf{y}) dV,$$

and  $\nabla^2 \psi_j + \left(\frac{\omega_j}{c}\right)^2 \psi_j = 0$  in  $V$ , and  $\nabla_{\perp} \psi_j = 0$  on  $S$ .

The acoustic field in the domain results from the superposition of each and every natural eigenmodes of the cavity driven by the source  $\mathcal{S}$ .

The expression of the modal amplitudes  $\hat{\eta}_j$  gives

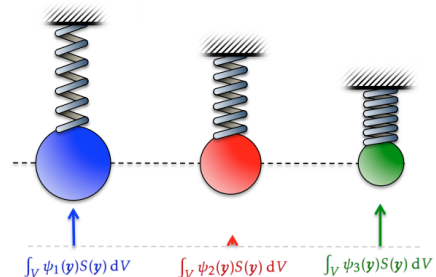
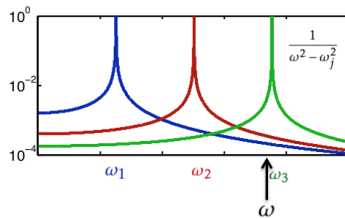
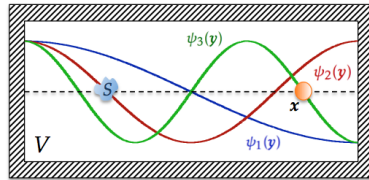
$$\left((i\omega)^2 + \omega_j^2\right) \hat{\eta}_j = -\frac{c^2}{V\Lambda_j} \int_V \psi_j(\mathbf{y}) S_\omega(\mathbf{y}) dV$$

and therefore the modal amplitudes  $\eta_j$  are governed by the following differential equations:

$$\frac{d^2 \eta_j}{dt^2} + \omega_j^2 \eta_j = -\frac{c^2}{V\Lambda_j} \int_V \psi_j(\mathbf{y}) S_\omega(\mathbf{y}) dV e^{i\omega t}$$

These are equations of harmonically forced oscillators.

## Galerkin expansion (4/4)



- From  $P(\mathbf{x}, \omega) = \sum_{j=1}^{\infty} \hat{\eta}_j(\omega) \psi_j(\mathbf{x})$ , one can see that the field at the listener position  $\mathbf{x}$  will depend on the eigenmodes at that position. Even if the source  $\mathcal{S}$  efficiently drives the mode  $\psi_n$ , we will not hear any contribution from that mode at its acoustic pressure nodes. The listener at position  $\mathbf{x}$  on the sketch can “hear” mode  $\psi_1$  and  $\psi_2$  but not  $\psi_3$ , no matter what their respective amplitudes are in the chamber.
- One can also see that to be effective in driving acoustic mode  $\psi_k$ , the source must be distributed in a region of the domain  $V$  where that mode can be excited. As an extreme case again, if the source is located at a node of  $\psi_k$ , the integral  $\int_V \psi_k(y)S(y) dV$  vanishes, and no matter how strong is  $\mathcal{S}$ , this mode will not be active anywhere in  $V$  ↳ The driving potential from a distributed source is weighted by its location with respect to the mode shapes. On the sketch, the source can be an efficient driver of modes  $\psi_1$  and  $\psi_3$ , but will be very weak in exciting mode  $\psi_2$  (look also at the mass spring system analogy).
- Even if the source is well located with respect to a given mode shape  $\psi_n$ , its amplitude will depend on the driving frequency  $\omega$  of the source. Indeed, the term  $(\omega^2 - \omega_n^2)^{-1}$  in the expression for the modal amplitude  $\hat{\eta}_n$  will be very small if  $\omega$  is far from  $\omega_n$ . A forced oscillator does not respond much if it is driven far away from its resonance frequency. On the other hand, for this idealized model, which does not contain damping terms, the response

## Field independent source

Imagine that the frequency  $\omega$  of the external harmonic forcing imposed by the source is close to one of the eigenfrequency of the cavity  $\omega_n$ . The contribution of the other modes will be negligible and the field can be expressed as

$$p'(\mathbf{x}, t) = P(\mathbf{x}, \omega) e^{i\omega t} \simeq \psi_n(\mathbf{x}) \dot{\eta}_n(\omega) e^{i\omega t} \quad \text{with}$$

$$\frac{d^2\eta_n}{dt^2} + \omega_n^2 \eta_n = -\frac{c^2}{V\Lambda_n} \int_V \psi_n(\mathbf{y}) S(\mathbf{y}) dV e^{i\omega t},$$

which is the equation of a forced oscillator driven by the source weighted by the mode shape  $\psi_n$ . In reality, there are always acoustic energy losses at the boundaries or in the volume and the response will not be infinite even if  $\omega = \omega_n$ . We can account for this dissipation by including a damping term in the modal amplitude equation, which then takes the following form

$$\ddot{\eta}_n + 2\alpha_n \dot{\eta}_n + \omega_n^2 \eta_n = F \cos(\omega t)$$

If the forcing is performed at a frequency which is close to the resonance frequency, and the damping is weak (underdamped oscillator), the modal amplitude of the source-driven cavity eigenshape  $\psi_n$  will be:

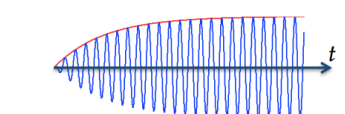
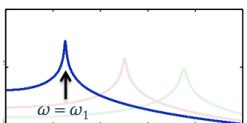
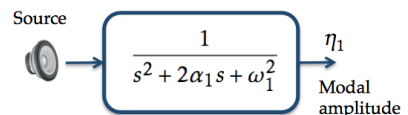
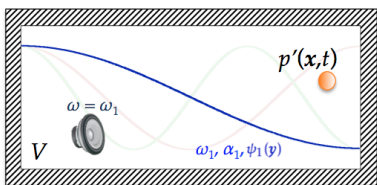
$$\eta_n(t) \sim \frac{F}{2\alpha_n \omega_n} (e^{-\alpha_n t} - 1) \sin(\omega_n t)$$

- Note that we assume here that eigenfrequencies of interest are far from each other, which means that the modal density is not high. In other words, at the frequency  $f = \omega/2\pi$  which is considered, the Helmholtz number  $\omega L/c$  associated with the cavity characteristic dimension  $L \sim V^{1/3}$ , is not too high.
- It could be possible to have an explicit expression of the damping induced by finite impedance at the walls if we would have carried with us the surface integrals in the Kirchhoff-Helmholtz equation.

# Field independent source

Let's imagine that the harmonic source is suddenly switched on and drives the acoustic field at a frequency close to  $\omega_1$ . Then, there will be a transient followed by the steady state response:

$$p'(x, t) \simeq \eta_1(t)\psi_1(x) = \frac{F}{2\alpha_1\omega_1} (e^{-\alpha_1 t} - 1) \sin(\omega_1 t)\psi_1(x)$$



$$p'(x, t) \simeq \eta_1(t)\psi_1(x) = \frac{F}{2\alpha_1\omega_1} (e^{-\alpha_1 t} - 1) \sin(\omega_1 t)\psi_1(x)$$

# Field dependent source

There are situations in which the source is itself influenced by the local acoustic field. In other words, there is a feedback loop induced by a two-way interaction between the acoustic field established in the cavity and the source.

We take again the situation where the resulting field can be well approximated by a single dominant eigenmode:  $p'(\mathbf{x}, t) \simeq \eta_n(t)\psi_n(\mathbf{x})$ . The source is a function of the local acoustic pressure, which is proportional to  $\eta_n$ , and/or to the acoustic velocity, which is proportional to  $\dot{\eta}_n$  in the case of harmonic oscillation.

For example, a **punctual source at  $\mathbf{x}_0$**  being **proportional** to the **local acoustic velocity at earlier time  $t - \tau$** , which means that the source responds to the acoustic field with a delay, is expressed as  $\mathcal{S} = G\dot{\eta}_n e^{-i\omega\tau} \delta(\mathbf{x}_0 - \mathbf{y})$ . In that case, the modal amplitude equation becomes

$$\frac{d^2\eta_n}{dt^2} + 2\alpha_n \frac{d\eta_n}{dt} + \omega_n^2 \eta_n = -\frac{c^2}{V\Lambda_n} \int_V \psi_n(\mathbf{y}) G e^{-i\omega\tau} \frac{d\eta_n}{dt} \delta(\mathbf{x}_0 - \mathbf{y}) dV$$

which gives the following ODE describing the modal amplitude

$$\underbrace{\ddot{\eta}_n + (2\alpha_n + 2\beta_n e^{-i\omega\tau}) \dot{\eta}_n + \omega_n^2 \eta_n}_{\text{Resistance}} = 0 \quad \text{with} \quad \beta_n = \frac{c^2 \psi_n(\mathbf{x}_0)}{2V\Lambda_n} G$$

- This happens for instance with aero- and thermo-acoustic sources and it yields high amplitude self-sustained oscillations of the acoustic field, which will be discussed in the next lectures.

# Field dependent source

The equation governing the modal amplitude is the equation for a damped harmonic oscillator. The corresponding complex resistance is given by

$$2\alpha_n + 2\beta_n(\cos \omega\tau - i \sin \omega\tau)$$

In acoustics, it is in general valid to assume lightly damped harmonic oscillations which corresponds to  $\alpha_n \ll \omega_n$  and  $\beta_n \ll \omega_n$ . In this case, the imaginary part of the resistance will result in a slight modification of the oscillation frequency and can be neglected.

However, the stability of such acoustic system will be dramatically influenced by the real part of the resistance  $2\nu_n = 2(\alpha_n + \beta_n \cos \omega\tau)$ . Indeed the characteristic polynomial is

$$\Omega^2 + 2\nu_n\Omega + \omega_n^2 = 0 \quad \text{with} \quad \nu_n \ll \omega_n \quad \rightsquigarrow \quad \Omega = -\nu_n \pm i\omega_n,$$

and the solution for the modal amplitude are

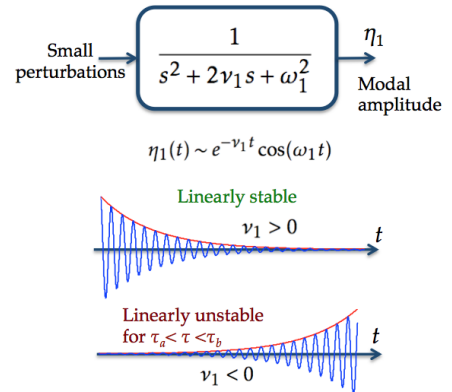
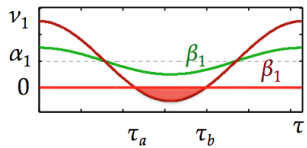
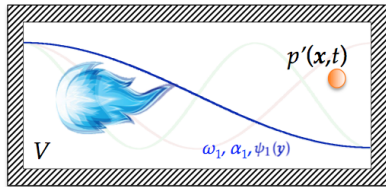
$$\eta_n(t) \sim e^{-\nu_n t} \cos(\omega_n t)$$

- If the source reacts to the local acoustic field such that  $\nu_n < 0$ , then the acoustic mode amplitude exponentially grows. This happens when (i) the absolute value of the source gain  $|\beta_n|$  is higher than the natural acoustic dissipation  $\alpha_n$  and when (ii) the source responds to the acoustic field within certain ranges of the delay  $\tau$ .

It corresponds to the case of a “negative” resistance and yields to thermo- or aero-acoustic instabilities.

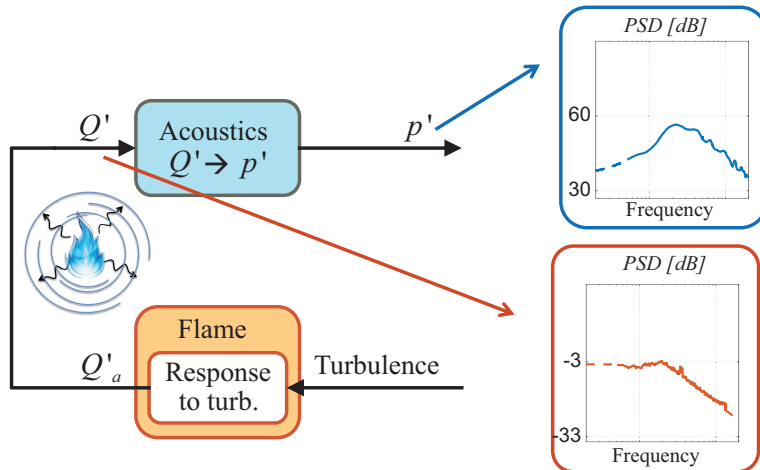
In such situation, the amplitude is limited at a certain level by nonlinear mechanisms which are not included in this model. The acoustic mode is then self-sustained and oscillates on a limit-cycle.

# Field dependent source



# Noise-driven thermoacoustic systems

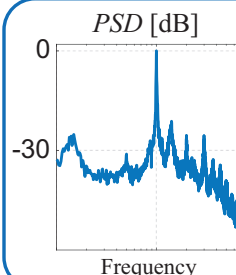
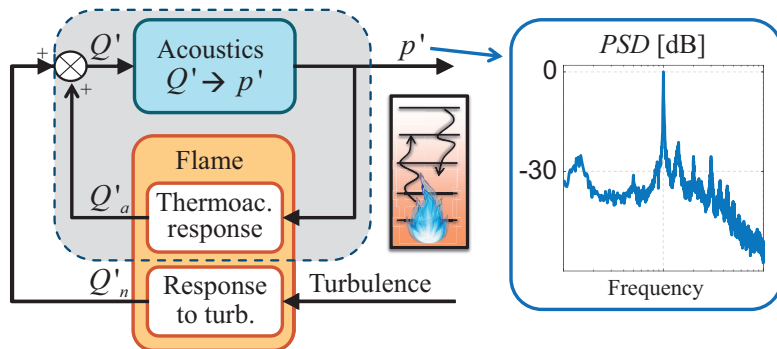
## 1) Open flame sound radiation



- Consider an unsteady heat source (flame) in an unconfined environment. The flow that supplies the source is turbulent and causes non-coherent fluctuations of the heat release rate, leading to a broadband pressure signal
- Note that a steady flame does not lead to pressure fluctuations. This is because the source term in the acoustic wave equation is proportional to the partial time derivative of the *unsteady* heat release rate  $\partial Q'/\partial t$
- Note that a steady flame does not lead to pressure fluctuations. This is because the source term in the acoustic wave equation is proportional to the *unsteady* heat release rate  $\partial Q'/\partial t$
- Shown to the left is the Power Spectral Density (PSD) of the heat release rate and the acoustic pressure. We see that in the region where the heat release rate is approximately constant, the acoustic pressure increases linearly with frequency, which in the frequency domain corresponds to applying the partial time derivative to  $Q$

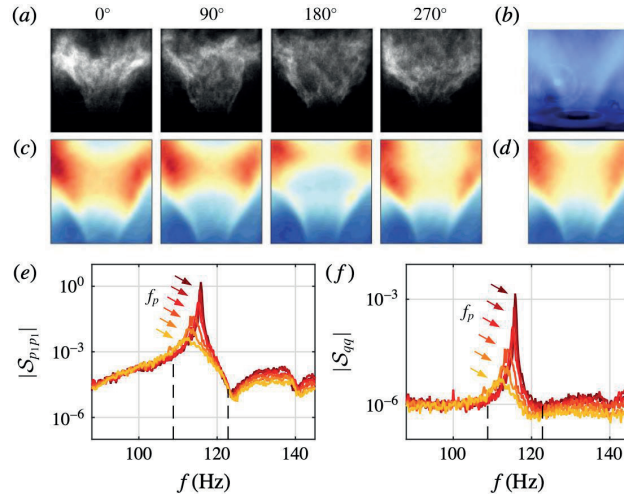
# Noise-driven thermoacoustic systems

## 2) Enclosed flame



- If we now put the flame in an enclosure, there is acoustic energy reflected back to the flame from the boundaries of the combustor. This creates a feedback loop leading to coherent fluctuations of the heat release rate
- The acoustic field in the enclosure is forced by the coherent (deterministic) and a turbulent (stochastic) parts of the unsteady heat release rate
- As we see on the left, the resulting PSD of the acoustic pressure is now a combination of resonances, which are most pronounced at low and intermediate frequencies and a low-pass broadband decay at high frequencies which is typical of turbulence-generated noise
- Resonance peaks correspond to thermoacoustic instabilities which occur at certain fundamental frequencies and their higher harmonics, where they are less pronounced
- The occurrence of instabilities depends on the location of the flame with respect to the acoustic modes of the enclosure and the response of the flame to acoustic perturbations

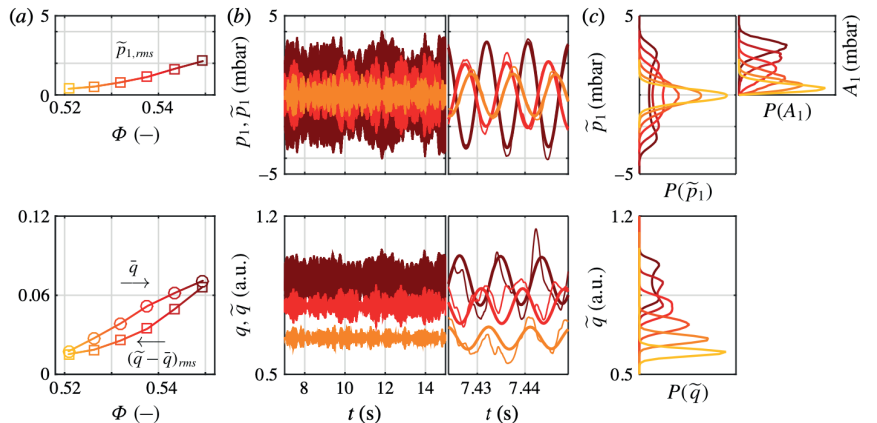
# Example 1: Chemiluminescence and PSDs



Boujo et al., JFM 2016

- To the left, we see (a) Snapshots of OH\* chemiluminescence at different phases of one acoustic period, and (b) direct visualisation of the time-averaged flame. (c) Phase-averaged and (d) time averaged OH\* chemiluminescence. (e) Power spectral density of acoustic pressure and (f) heat release , for different equivalence ratios  $\Phi = 0.521$  (light), 0.549 (dark).
- If we look at (e) and (f), we see a peak in the PSD of the acoustic pressure which grows with increasing equivalence ratio. This peak corresponds to a thermoacoustic instability
- The acoustic pressure signal is measured with microphones in the combustor. The heat release rate is inferred from the measured light intensity, which is proportional to the heat release rate (not always true)

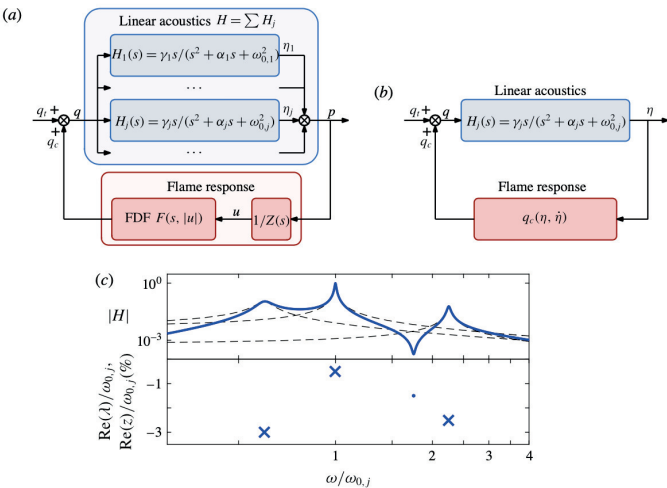
# Example 1 (continued): Acoustic pressure time series and PDFs



Boujo et al., JFM 2016

- To the left, we see (a) Mean and root mean square of the acoustic pressure and heat release rate filtered around the main peak frequency vs. fuel-air equivalence ratio  $\Phi$ .
- (b) Samples of the 180 s acoustic pressure and heat release signals for different equivalence ratios  $\Phi = 0.526, 0.538, 0.549$ : original signals of the acoustic pressure and the heat release (thin lines) and filtered signals (thick lines).
- (c) PDF of the filtered acoustic pressure, of its envelope, and of the filtered heat release
- We see that the RMS values of the acoustic pressure, the mean heat release rate and the heat release fluctuations increase with increasing equivalence ratio
- We see that the RMS values of the acoustic pressure, the mean heat release rate and the heat release fluctuations increase with increasing equivalence ratio
- In (c), we see the PDF of the acoustic pressure and its amplitude. From this we see well the bimodal distribution which corresponds to the limit cycle that appears when the equivalence ratio is increased. When there is only a single peak of the acoustic pressure, this means that the system is linearly stable. We see this change from a unimodal to a bimodal distribution also in the PDF of the heat release rate, while the mean heat release grows

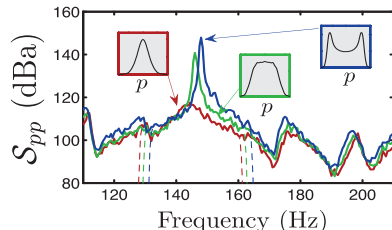
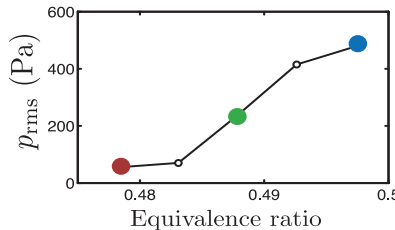
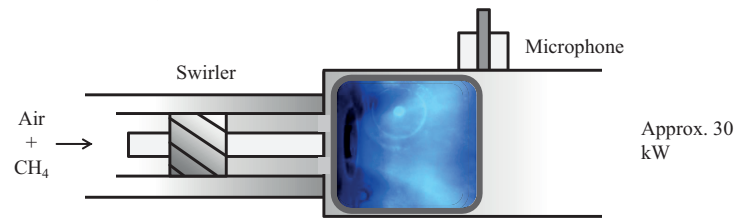
# Example 1 (continued): Low-order modelling of thermoacoustic instabilities



- In this lecture, we focus on the low-order modelling of thermoacoustic instabilities and the statistical behavior of the acoustic pressure. This means we will not look at the flame transfer function in detail, but incorporate some important effects of it in a low-order model
- This low-order approach is an important step towards the more detailed analysis with thermoacoustic networks
- To the left, we see an example of a comparison between (a) a detailed thermoacoustic network describing several acoustic modes with a measured (or simulated) flame transfer function and (b) a low-order model which describes a single mode and a simple flame response function which depends on the modal amplitude of the acoustic mode of interest
- A key assumption we always make is that the mode shape of the thermoacoustic modes is not very different from the unforced acoustic modes of the enclosure. These acoustic eigenmodes form an orthogonal basis onto which we can project our system dynamics, which is the basis of our approach

## Example 2 (continued): Experimental setup - Context

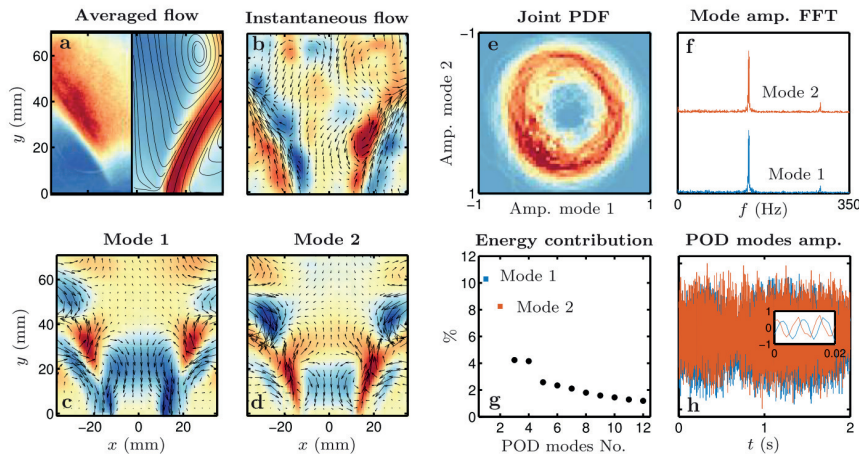
Noiray and Denisov, PROCI 2017



- We see to the left: as the equivalence ratio is increased a thermoacoustic instability appears from a supercritical Hopf bifurcation
- The instability leads to a limit cycle, which is quantified by the acoustic pressure signal time traces and the corresponding PDFs shown in the bottom right figure
- Note that the pressure signal should be filtered around the peak of interest to increase signal quality
- The top figure of the flame shos
- Movie 5

## Example 2: Flow field

Noiray and Denisov, PROCI 2017



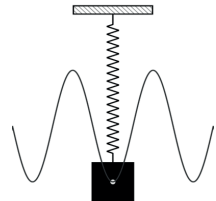
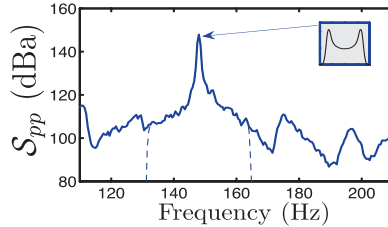
- (a) Averaged axial velocity (right) from  $-8$  (blue) to  $15$  m/s (red) and OH\* chemiluminescence (left) at self-oscillating condition (control switched-off). (b) instantaneous vorticity field from  $-3800$  (blue) to  $3800$   $\text{s}^{-1}$  (red). (c-d) POD modes 1 and 2, blue and red for negative and positive axial displacement. (e) Joint PDF of POD modes amplitudes from 2 s data (294 acoustic cycles). (f) Fourier transform of the POD modes amplitudes. (g) Energy contribution of the first 12 POD modes. (h) Temporal evolution of the amplitudes of modes 1 and 2 (the inset indicates the corresponding 90deg phase shift)
- High velocity flow (jet of air-methane mixture) is supplying the flame. The hot products recirculate toward the root of the flame in the inner recirculation zone. There also is an outer recirculation zone which stabilizes the flame
- From proper orthogonal decomposition (POD), we obtain the dominant modes 1 and 2, which are the coherent fluctuations of the velocity field which, when they are convected, cause the coherent fluctuations of the heat release rate
- Since the flame dimensions are much smaller than the acoustic wavelength, we can assume that the flame is compact → the local fluctuations of the acoustic pressure are uniform across the flame (not true at high frequencies)

# Low order model of the thermoacoustic coupling

Dominant mode → modal projection  
 $p(t, x) \simeq \eta(t)\psi(x)$

Harmonic oscillator

$$\ddot{\eta} + \omega^2 \eta = 0$$



- As shown on the left, we "expand" the acoustic pressure in terms of mode shapes, but we only keep one (dominant) mode
- This means that the acoustic pressure is equal to the acoustic eigenmode  $\psi(x)$ , modulated by the time-dependent modal amplitude  $\eta(t)$
- Without including any damping in this model, this leads to a harmonic oscillator equation with eigenfrequency equal to that of the acoustic eigenmode  $\psi(x)$
- This approach, which is only sketched here, will be discussed in more detail in the coming lectures

# Low order model of the thermoacoustic coupling

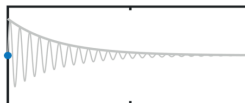
Dominant mode → modal projection

$$p(t, x) \simeq \eta(t)\psi(x)$$

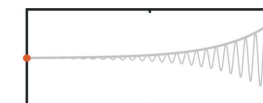
Damped harmonic oscillator

$$\ddot{\eta} + \omega^2\eta = 2\nu\dot{\eta}$$

Linear damping and driving mechanisms at  $f = \omega/2\pi$  from acoustic-flow, acoustic-flame, acoustic-structure interactions



$\nu < 0 \rightsquigarrow$  linearly stable



$\nu > 0 \rightsquigarrow$  linearly unstable

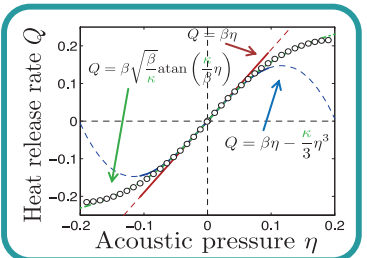
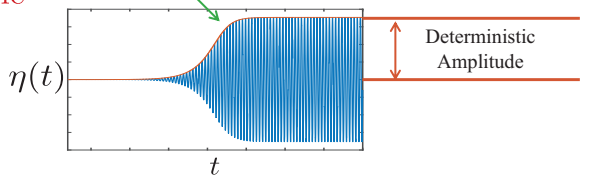
- We now refine this model by including acoustic-flow, acoustic-flame and acoustic-structure interactions
- We do this by including a damping term  $2\nu\dot{\eta}$  which determines the linear stability of the system
- Depending on the sign of  $\nu$ , the acoustic pressure will grow ( $\nu > 0$ ) or decrease ( $\nu < 0$ )
- Note that the oscillation under the envelope occurs at a much smaller time scale than the exponential growth of the amplitude. This is because the damping term  $\nu$  is much smaller than  $\omega$  (eigenfrequency of  $\psi$ )
- With this addition, we have described the linear stability of the thermoacoustic system. This approach is valid only before near the bifurcation point, when the acoustic pressure (and hence the modal amplitude  $\eta$ ) is still small

# Low order model of the thermoacoustic coupling

Damped harmonic oscillator

$$\ddot{\eta} + \omega^2 \eta = \dot{\eta} (2\nu - \kappa \eta^2)$$

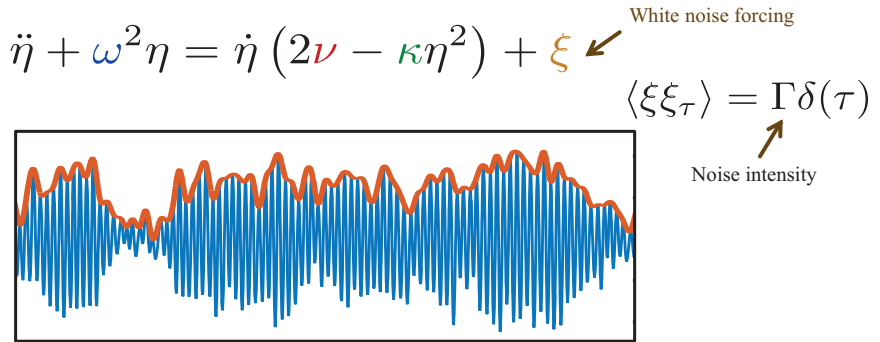
$\nu > 0 \rightsquigarrow$   
linearly unstable



- We see in practice that the exponential growth stops at some acoustic pressure amplitude, which defines a limit cycle (it's approximately a circle in the  $\eta$ - $\dot{\eta}$  plane). We now further refine our system to model this effect
- We do so by adding a negative cubic term to the relation between  $\eta$  and the heat release rate (dashed blue curve). Taking the time derivative leads to a term proportional to  $-\dot{\eta}\eta^2$  on the r.h.s., which corresponds to the classic Van der Pol oscillator
- Physically, this cubic term represents the heat release rate fluctuation caused by the flame feedback to the acoustic pressure. As we see in the inset to the left, we represent this heat as a function of the modal amplitude  $\eta$
- Note that also the cubic term is only valid in a neighborhood of the bifurcation point, or for intermediate modal amplitudes. At higher  $\eta$ , the acoustic pressure induces large-scale motions of the flame, and more complicated models are necessary to describe the relation between  $\eta$  and the heat release rate. Examples of such models will be discussed in more detail in the coming lectures
- It is important to remember that this approach and the typical limit cycle behavior we describe are only applicable when both  $\nu$  and  $\kappa$  are much smaller than  $\omega$ , so that we are in the lightly damped, weakly nonlinear regime. However, this is typically the case in practice

# Low order model of the thermoacoustic coupling

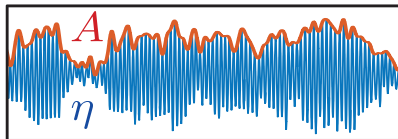
Turbulence induces non-coherent heat release rate which drives the self-sustained oscillations



- We observe in reality that the limit cycle is not a perfect circle in the  $\eta$ - $\dot{\eta}$  plane, but that there is a stochastic oscillation of the modal amplitude around the deterministic limit cycle amplitude
- This is due to the previously describe broadband stochastic forcing by the turbulent flow which supplies the flame. We now add another layer to our low-order model to incorporate these stochastic effects
- We achieve this by adding on the r.h.s. the stochastic white-noise forcing term  $\xi$  with noise intensity  $\Gamma$
- Our deterministic approach is now not applicable anymore, and we observe stochastic behavior in the time signal of  $\eta$ , with a slowly varying amplitude around the deterministic limit cycle amplitude. This confirms that our approach is correctly reproducing some key features of the phenomenon that we can also observe in practice

# Stochastic amplitude equation

$$\ddot{\eta} + \omega^2 \eta = \underbrace{\dot{\eta}(2\nu - \kappa\eta^2)}_{\text{Small compared to l.h.s.}} + \xi$$



Go to Amplitude-Phase coordinates with

$$\eta = A \cos(\omega t + \varphi)$$

$$\text{and } A = \sqrt{\eta^2 + (\dot{\eta}/\omega)^2}$$

Acoustic energy  $\propto A^2$

Deterministic and stochastic averaging

$$\dot{A} = A \left( \nu - \frac{\kappa}{8} A^2 \right) + \frac{\Gamma}{4\omega^2 A} + \zeta$$

- As we saw previously, we end up with the equation of a Van der Pol oscillator with stochastic forcing which describes the dynamics of  $\eta$ .
- We now take advantage of the fact that in thermoacoustics, the damping and nonlinear terms on the r.h.s. are typically much smaller than the l.h.s. This means that we will have weakly damped, quasi-sinusoidal oscillations
- In this situation, it is convenient to change to the amplitude-phase description using the coordinate transformation shown on the left. Taking this ansatz and performing deterministic and stochastic averaging, we obtain the amplitude equation shown on the bottom to the left
- We call this type of equation a Langevin equation
- Details of the stochastic averaging can be found in the lecture material (M. Scott, stochastic processes)
- Looking at the amplitude equation, we see that the l.h.s. is composed of a deterministic part,  $A(\nu - \frac{\kappa}{8} A^2) + \frac{\Gamma}{4\omega^2 A}$ , and a stochastic part  $\zeta$ . Remember that  $\Gamma$  is the noise intensity of the white noise forcing  $\xi$

# Nonlinear oscillator driven by additive white noise

$$\ddot{\eta} + \omega_0^2 \eta = f(\eta, \dot{\eta}) + \xi \quad \text{with} \quad \langle \xi \xi_\tau \rangle = \Gamma \delta(\tau)$$

If l.h.s.  $\ll$  r.h.s., adequate projection onto amplitude and phase

$$A = \sqrt{\eta^2 + (\dot{\eta}/\omega_0)^2} \quad \varphi = -\arctan\left(\frac{\dot{\eta}}{\omega_0 \eta}\right) - \omega_0 t$$

Which yields

$$\begin{aligned} \dot{A} &= \underbrace{-\frac{\sin \phi}{\omega_0} f(A \cos \phi, -A \omega_0 \sin \phi)}_{h_1(A, \phi)} - \underbrace{-\frac{\sin \phi}{\omega_0} \xi}_{h_2(A, \phi)} \\ \dot{\varphi} &= \underbrace{-\frac{\cos \phi}{A \omega_0} f(A \cos \phi, -A \omega_0 \sin \phi)}_{h_3(A, \phi)} - \underbrace{-\frac{\cos \phi}{A \omega_0} \xi}_{h_4(A, \phi)} \end{aligned}$$

- To the left, we sketch elements of the averaging process
- Taking the time derivative of the expressions for the amplitude  $A$  and the phase  $\phi$ , and substituting into it the oscillator equation, yields the two equations for  $\dot{A}$  and  $\dot{\phi}$  shown on the bottom

# Nonlinear oscillator driven by additive white noise

$$\begin{aligned}\dot{A} &= -\underbrace{\frac{\sin \phi}{\omega_0} f(A \cos \phi, -A \omega_0 \sin \phi)}_{h_1(A, \phi)} - \underbrace{\frac{\sin \phi}{\omega_0} \xi}_{h_2(A, \phi)} \\ \dot{\phi} &= -\underbrace{\frac{\cos \phi}{A \omega_0} f(A \cos \phi, -A \omega_0 \sin \phi)}_{h_3(A, \phi)} - \underbrace{\frac{\cos \phi}{A \omega_0} \xi}_{h_4(A, \phi)}\end{aligned}$$

Deterministic averaging

- Expansion for  $f$
- Integrate over an oscillation to get rid of fast terms



$$\begin{aligned}f(\eta, \dot{\eta}) &= \sum_n \sum_m \gamma_{n,m} \eta^n \dot{\eta}^m \\ \langle h_1 \rangle &= \frac{\gamma_{0,1}}{2} A + \left( \frac{\gamma_{2,1}}{8} + \frac{3\omega_0^2 \gamma_{0,3}}{8} \right) A^3 + \mathcal{O}(A^5) \\ \langle h_3 \rangle &= -\frac{\gamma_{1,0}}{2\omega_0} - \left( \frac{\omega_0 \gamma_{1,2}}{8} + \frac{3\gamma_{3,0}}{8\omega} \right) A^2 + \mathcal{O}(A^4)\end{aligned}$$

- On the terms  $h_1(A, \phi)$  and  $h_3(A, \phi)$ , we perform deterministic averaging as sketched to the left
- First we expand  $f$  into a Taylor series and then we integrate over one oscillation cycle to get rid of the fast terms
- This approach works for general functions  $f$ , provided we can express it as a Taylor series

# Nonlinear oscillator driven by additive white noise

$$\begin{aligned}\dot{A} &= -\frac{\sin \phi}{\omega_0} f(A \cos \phi, -A \omega_0 \sin \phi) \\ \dot{\phi} &= -\frac{\cos \phi}{A \omega_0} f(A \cos \phi, -A \omega_0 \sin \phi)\end{aligned}$$

$\overbrace{\hspace{10em}}^{h_1(A,\phi)}$        $\overbrace{\hspace{10em}}^{h_2(A,\phi)}$

$\overbrace{\hspace{10em}}^{h_3(A,\phi)}$        $\overbrace{\hspace{10em}}^{h_4(A,\phi)}$

Stochastic averaging

$$h_2(A, \phi) = \frac{\Gamma}{4\omega_0^2 A} + \zeta \quad h_4(A, \phi) = \frac{1}{A} \chi$$

$$\langle \chi \chi_\tau \rangle = \langle \zeta \zeta_\tau \rangle = \Gamma / 2\omega_0^2 \delta(\tau)$$

- Next, we perform deterministic averaging on the terms  $h_2(A, \phi)$  and  $h_4(A, \phi)$
- This leads to a deterministic contribution in the equation for  $\dot{A}$  which is inversely proportional to  $A$ , as well as stochastic contributions in the equations for both  $\dot{A}$  and  $\dot{\phi}$

# Nonlinear oscillator driven by additive white noise

$$\ddot{\eta} + \omega_0^2 \eta = f(\eta, \dot{\eta}) + \xi \quad \text{with} \quad \langle \xi \xi_\tau \rangle = \Gamma \delta(\tau)$$

Amplitude and Phase dynamics

$$A = \sqrt{\eta^2 + (\dot{\eta}/\omega_0)^2} \quad \varphi = -\arctan\left(\frac{\dot{\eta}}{\omega_0 \eta}\right) - \omega_0 t$$

$$\dot{A} = \frac{\gamma_{0,1}}{2} A + \left( \frac{\gamma_{2,1}}{8} + \frac{3\omega_0^2 \gamma_{0,3}}{8} \right) A^3 + \frac{\Gamma}{4\omega_0^2 A} + \zeta + \mathcal{O}(A^5)$$

$$\dot{\varphi} = -\frac{\gamma_{1,0}}{2\omega_0} - \left( \frac{\omega_0 \gamma_{1,2}}{8} + \frac{3\gamma_{3,0}}{8\omega} \right) A^2 + \frac{1}{A} \chi + \mathcal{O}(A^4)$$

- The resulting system of equations which we obtain from the averaging process, for a general function  $f$  is given to the left
- Why Taylor expansion for  $f$ ? → Because we are always talking about small perturbations  $\eta$  and  $\dot{\eta}$  of the total pressure. Even in the most extreme cases, the acoustic pressure caused by thermoacoustic instabilities will be about 5 percent of the mean pressure, which already leads to the mechanical failure of the system parts

# Amplitude potential and Fokker-Planck equation

Amplitude equation

$$\dot{A} = A \left( \nu - \frac{\kappa}{8} A^2 \right) + \frac{\Gamma}{4\omega^2 A} + \zeta$$

$\mathcal{F}(A) = -\partial\mathcal{V}/\partial A$

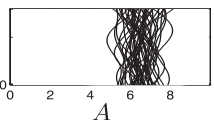
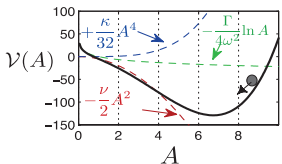
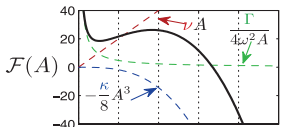
Potential

$$\mathcal{V}(A) = -\frac{\nu}{2} A^2 + \frac{\kappa}{32} A^4 - \frac{\Gamma}{4\omega^2} \ln A$$

Fokker-Planck equation

~~$$\frac{\partial}{\partial t} P_{A,t} = -\frac{\partial}{\partial A} (\mathcal{F}(A)P_{A,t}) + \frac{\Gamma}{4\omega^2} \frac{\partial^2}{\partial A^2} P_{A,t}$$~~

Stationary solution  $P_{A,\infty} = \mathcal{N} \exp \left( -\frac{4\omega^2}{\Gamma} \mathcal{V}(A) \right)$



- How can we relate our approach so far to the acoustic pressure statistics that we saw in the beginning of the lecture?
- First, we note that we can write the deterministic part of the amplitude equation as the derivative of a potential with respect to  $A$
- The figures to the left show the typical shape of the various contributions to this potential. Note that the deterministic contribution from the stochastic forcing leads to a term that is infinite at zero amplitude. This means that this term will always force the system away from  $A = 0$
- The bottom plot shows typical behavior of  $A$  over time. We observe a stochastic fluctuation around a deterministic limit cycle amplitude
- Note that it is always possible to express an univariate Langevin equation in terms of a potential

# Amplitude potential and Fokker-Planck equation

Amplitude equation

$$\dot{A} = A \left( \nu - \frac{\kappa}{8} A^2 \right) + \frac{\Gamma}{4\omega^2 A} + \zeta$$

$\mathcal{F}(A) = -\partial\mathcal{V}/\partial A$

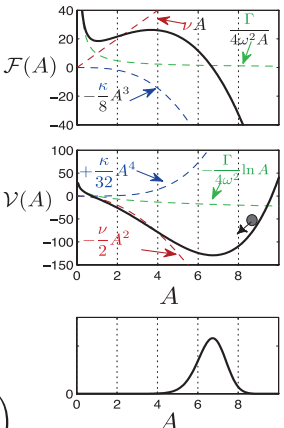
Potential

$$\mathcal{V}(A) = -\frac{\nu}{2} A^2 + \frac{\kappa}{32} A^4 - \frac{\Gamma}{4\omega^2} \ln A$$

Fokker-Planck equation

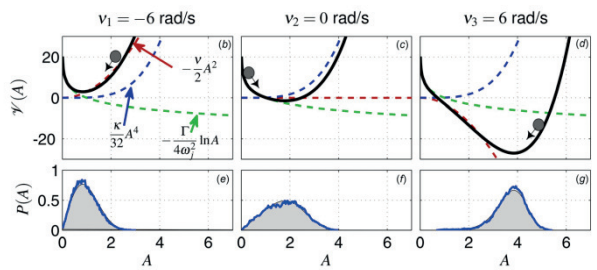
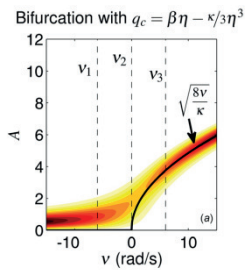
~~$$\frac{\partial P_{A,t}}{\partial t} = -\frac{\partial}{\partial A} (\mathcal{F}(A)P_{A,t}) + \frac{\Gamma}{4\omega^2} \frac{\partial^2}{\partial A^2} P_{A,t}$$~~

Stationary solution  $P_{A,\infty} = \mathcal{N} \exp \left( -\frac{4\omega^2}{\Gamma} \mathcal{V}(A) \right)$



- How can we relate our approach so far to the acoustic pressure statistics that we saw in the beginning of the lecture?
- First, we note that we can write the deterministic part of the amplitude equation as the derivative of a potential with respect to  $A$
- The figures to the left show the typical shape of the various contributions to this potential. Note that the deterministic contribution from the stochastic forcing leads to a term that is infinite at zero amplitude. This means that this term will always force the system away from  $A = 0$
- The bottom plot shows typical behavior of  $A$  over time. We observe a stochastic fluctuation around a deterministic limit cycle amplitude
- This stochastic behavior can be described by the probability density function  $P_{A,t}$ , which gives the probability of the amplitude being equal to  $A$  at time  $t$
- The evolution of  $P_{A,t}$  is given by the Fokker-Planck equation associated with the amplitude equation
- In the stationary case, this Fokker-Planck equation has an explicit solution which describes the hill-shaped probability distribution around the deterministic limit cycle amplitude that we observe

# Example: Bifurcation diagram



Noiray, JEGTP, 2017

- Stochastic bifurcation diagram associated with the acoustic amplitude dynamics. The bifurcation parameter is the growth rate  $v$ . A contour plot of the theoretical probability density function (p.d.f.)  $P(A)$  is shown together with the deterministic bifurcation curve (solid line). (e)–(g)  $P(A)$  at selected linear growth rates  $v_i$  with a variation from linearly stable ( $v < 0$ ) to linearly unstable ( $v > 0$ ) conditions. The shaded areas are the theoretical p.d.f., and the thick blue lines correspond to the p.d.f. from the normalized histograms of the simulated stochastic Van der Pol oscillators. (b)–(d) Corresponding potential and related contributions.
- Looking at the bifurcation diagram, we see that in the linearly stable regime ( $v < 0$ ), the amplitude oscillates around 0, as expect from the deterministic contribution from the stochastic forcing. The red curve is pointing up, shifting the potential valley close to  $A = 0$ . This behavior is also reflected by the p.d.f. shown for  $v_1$ .
- In the marginally stable case ( $v_2$ ), we are right around the bifurcation point. In this case, the red curve is more or less straight, which causes the potential valley to shift from 0 to intermediate values of  $A$ .
- At  $v_3$ , we observe a limit cycle. In this case, the red curve goes to  $-\infty$ , which shifts the potential valley to larger  $A$ .
- Lecture material → MATLAB script to reproduce the results shown here

# Contents

1 Thermoacoustic networks

2 Low order modelling

3 Limit cycle amplitude dynamics

4 Super- and subcritical Hopf bifurcation

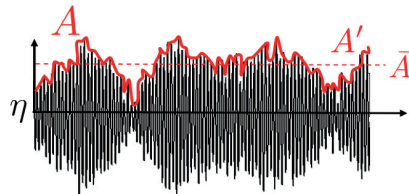
# Limit cycle amplitude dynamics

$$\ddot{\eta} + \omega_0^2 \eta = \underbrace{\dot{\eta}(\nu - \kappa\eta^2)}_{\text{Small compared to l.h.s}} + \xi$$

Go to Amplitude-Phase coordinate with  
 $\eta = A \cos(\omega_0 t + \varphi)$   
and  $A = \sqrt{\eta^2 + (\dot{\eta}/\omega_0)^2}$

Deterministic+stochastic averaging

$$\dot{A} = A \left( \nu - \frac{\kappa}{8} A^2 \right) + \frac{\Gamma}{4\omega_0^2 A} + \zeta$$



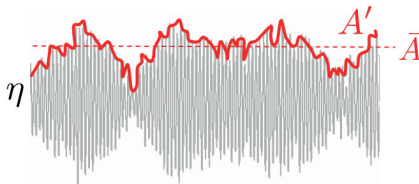
Amplitude equation linearized around mean amplitude with  
 $A' \ll \bar{A}$  and  $\bar{A} \approx A_0 = (8\nu/\kappa)^{1/2}$

$$\dot{A}' \simeq -2\nu A' + \zeta$$

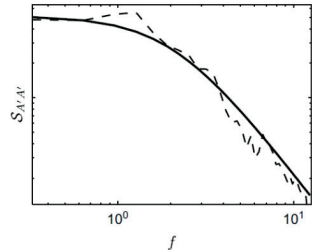
with  $\langle \zeta \zeta_\tau \rangle = \frac{\Gamma}{2\omega_0^2} \delta(\tau)$

- We now look at the transition region around the bifurcation point. Specifically, we are interested in the fluctuations of the amplitude  $A'$  in this region
- Recall that we derived the equation for  $\dot{A}$  shown to the left by deterministic and stochastic averaging of the oscillator ODE for  $\eta$
- First, we assume that we have a linearly unstable system  $\nu > 0$ . By linearizing the ODE for  $\dot{A}$  around the deterministic limit cycle amplitude  $A_0 = (8\nu/\kappa)^{1/2}$ , we obtain a first-order ODE for the amplitude fluctuations  $A'$ , shown in the blue box at the bottom right in the picture to the left

# Limit cycle amplitude dynamics



$$\dot{A}' \simeq -2\nu A' + \zeta$$

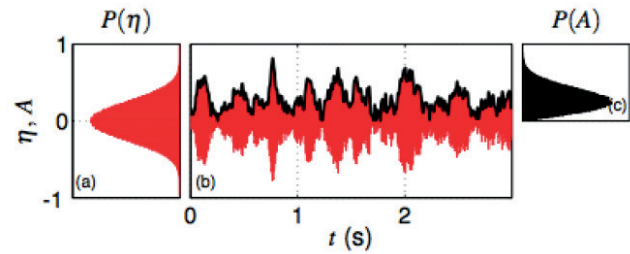
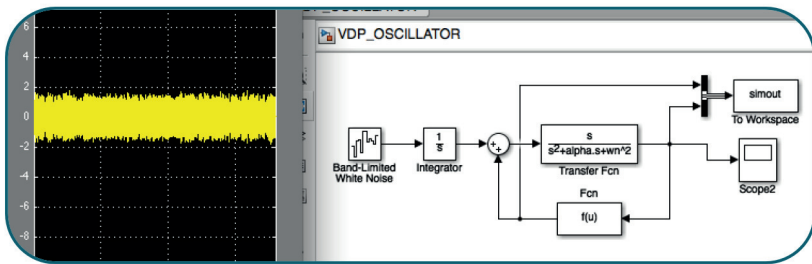


$$\mathcal{S}_{A'A'}(\omega) = \frac{1}{\omega^2 + 4\nu^2} \mathcal{S}_{\zeta\zeta}$$

The growth rate is half the cut-off frequency of the envelope power spectral density

- Neglecting the stochastic term, this equation has exponentially decaying solutions, because  $\nu > 0$ . This means that after a small perturbation, the amplitude  $A$  will revert back to the deterministic limit cycle amplitude. At the same time, there is a stochastic forcing term  $\zeta$  on the RHS which will always cause such small perturbations in  $A'$ , leading to the behavior of  $A'$  sketched in the plot on the left (red line)
- If we look at the equivalent of this first-order ODE in the frequency domain, we find that the system behaves like a first-order low pass filter with a characteristic cut-off frequency which is equal to  $2\nu$ , i.e., two times the linear growth rate
- This means that the fluctuations  $A'$ , in a neighborhood of the Hopf bifurcation point, the cut-off frequency will get smaller and smaller as we approach the bifurcation point. This means that the correlation time of the perturbations will get bigger and bigger, leading to very slow modulations of the amplitude near the bifurcation
- In contrast, far away (to the right) from the bifurcation point, with a large positive  $\nu$ , we get a first-order filter with a larger cut-off frequency. This is due to the fact that the closer we get to the bifurcation point, the more our oscillator behaves like an undamped oscillator, which has an infinitely large correlation time

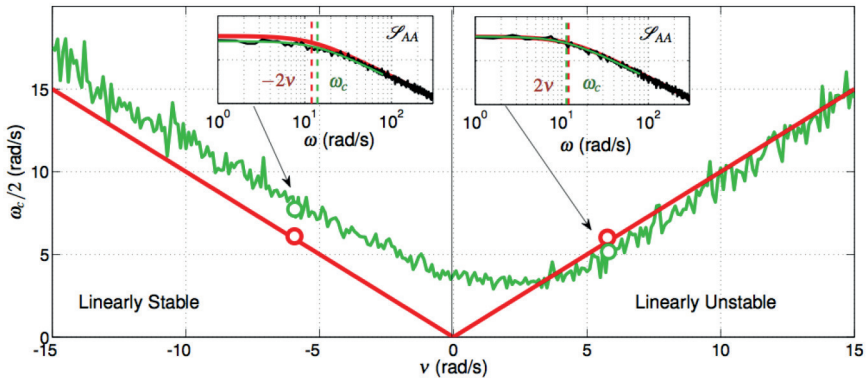
# Limit cycle amplitude dynamics



- It can be shown that this is also valid for the linearly stable case and therefore  $|v| = \omega_c/2$
- To validate this result, a simulink model of the stochastic Van-der-Pol oscillator is used
- Based on the MATLAB script you received in the learning material 2 weeks ago, you can investigate this behavior yourself
- By changing  $\beta$  in the feedback function (the flame response), you can generate different time traces. From these, you obtain the amplitude envelope, from which you can compute the PSD of the envelope

# Limit cycle amplitude dynamics

$$|v| = \omega_c/2$$



- The result of such an analysis is shown in the figure to the left. We see that if we compute the PSD in the unstable regime, it looks like a low pass filter with cut-off frequency  $\omega_c = 2\nu$ .
- In the paper, you also find the derivation of the equivalent result for the linearly stable case. In that situation, we find exactly the same equation for  $A'$ , given by

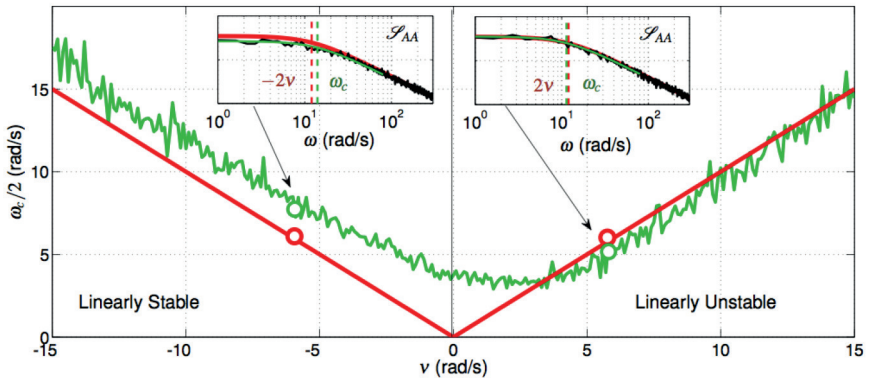
$$\dot{A}' = 2\nu A + \zeta \quad (7)$$

with  $\nu < 0$ . In this case, also, the cutoff frequency is equal to  $-2\nu$ .

- Shown in the figure to the left, is the result of time domain simulations (green), compared with the predictions (red) of the model. Specifically, at each value of the growth rate  $\nu u$ , from time domain simulations, the cut-off frequency of the PSD of the amplitude fluctuations is computed, resulting in the green curve you see to the left
- This result provides us with a method to identify from experiments the growth rate in the vicinity of the bifurcation as a function of another bifurcation parameter, e.g., the temperature

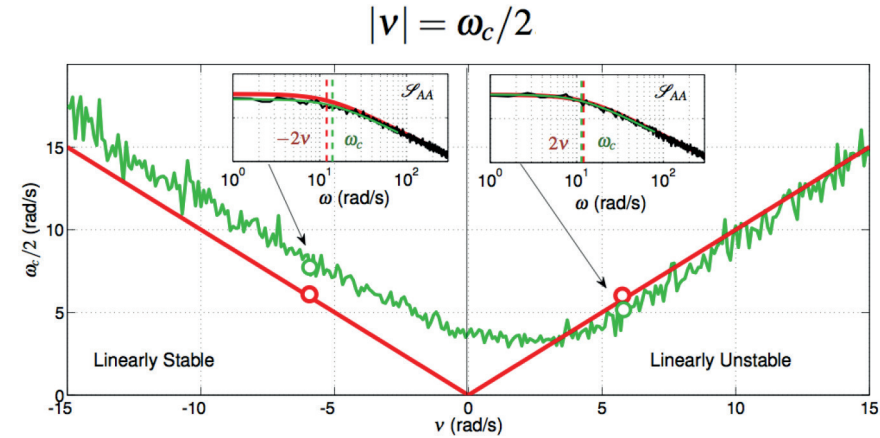
# Limit cycle amplitude dynamics

$$|v| = \omega_c/2$$



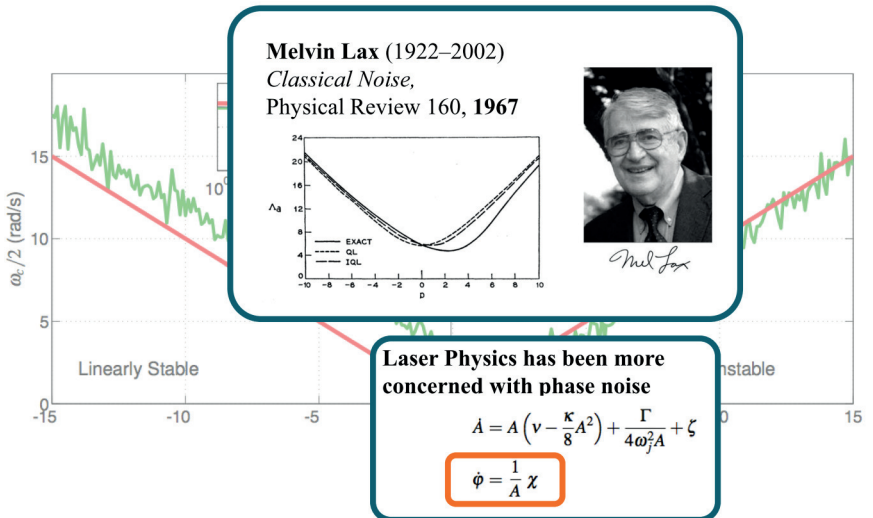
- Also, by monitoring the cut-off frequency of the PSD of the signal envelope, you can monitor how far you are from bifurcation point. By continuously recording the signal, processing its envelope to get the PSD and identifying the cut-off frequency, the stability margin can be monitored to protect the system from an instability
- The critical slowing-down behavior near the bifurcation point is typical of many systems before a sudden change in the system behavior
- One limitation regarding the possibility of monitoring the margin of stability of the system is the existence of a second significant peak in the PSD of the acoustic pressure, corresponding to a second significant acoustic mode. In this case, we would have to band-pass filter the signal near each of the peaks and determine their stability margins separately. This is because the result we discuss here was derived using a unimodal expansion of the acoustic pressure
- Another limitation is the size of the growth rate  $v$ , as this approach is only valid in the vicinity of the bifurcation where  $v$  is very small. Far away from the bifurcation point in the unstable regime this method will not be valid anymore

# Limit cycle amplitude dynamics



- A third limitation of the approach is that in the derivation of the result, the assumption  $A' \ll \bar{A}$  was made, which is not valid near the bifurcation point and also less valid in the stable regime than in the unstable regime, which explains the discrepancies between the simulations (green) and the prediction (red) that we see in the figure to the left. This also explains why there is such good agreement in the unstable regime: There, the mean amplitude  $\bar{A}$  is much larger than the fluctuations  $A'$ , and the assumption  $A' \ll \bar{A}$  is always valid

# Limit cycle amplitude dynamics



- A similar result is valid also for other types of oscillators. The critical slowing-down was first pointed out by Melvin Lax in a classic paper in Physical Review. He was more interested in Laser physics, where there is also a Hopf bifurcation and a slowing-down. There, he was more concerned with phase noise, which we didn't look at here
- In any case, many extensions of the result we just discussed can be found for various physical systems. The result on the linearly stable case is true for any oscillator, while the slope in the stable regime depends on the type of nonlinearity we are looking at

# Contents

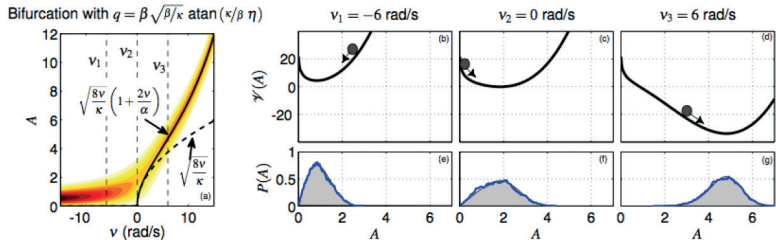
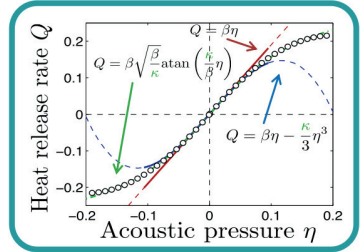
1 Thermoacoustic networks

2 Low order modelling

3 Limit cycle amplitude dynamics

4 Super- and subcritical Hopf bifurcation

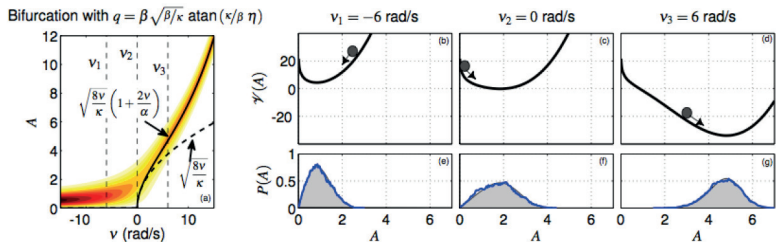
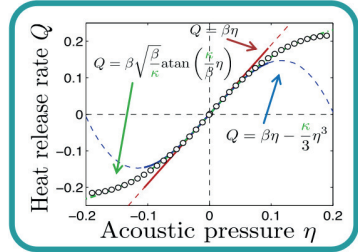
# Super- and subcritical Hopf bifurcation



Noiray, JEGTP 2017

- Now, let's look at other types of nonlinearities. What we've seen so far is the Van-der-Pol oscillator, which is based on an approximation of the system nonlinearities by a cubic function of  $\eta$
- In the figure to the left, the dots correspond to an experimentally measured heat release rate. We see in the figure that the cubic approximation is valid up to a certain value of the modal amplitude. After that point, the two curves diverge
- This means that if we have fluctuations which exceed a certain value, then the Van-der-Pol equation will not be able to quantitatively capture the system
- Another function which can be used to approximate the heat release rate is the arctangent function shown in the figure, with the 2 parameters  $\beta$  and  $\kappa$ . We see that the arctangent can accurately reproduce the experimental results over all modal amplitudes we considered
- Such a sigmoid-type saturation at the fundamental frequency is typical of many physical systems

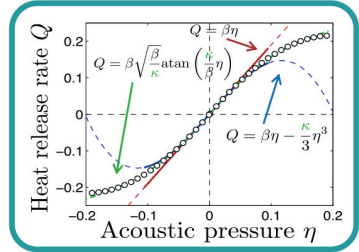
# Super- and subcritical Hopf bifurcation



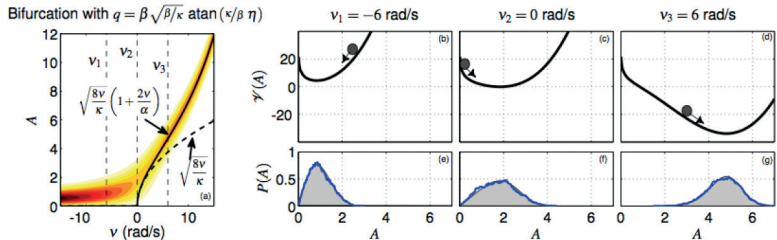
Noiray, JEGTP 2017

- If we plug the arctangent formulation into our oscillator equation, we get a different evolution of the deterministic mean amplitude, which is shown in the plot on the bottom left
- The new bifurcation curve we get is a diverging curve which coincides with the one from the cubic approximation for small  $v$
- If stochastic forcing is included in the model, the black-red-yellow colored region indicates the probability density function as a function of the growth rate. Qualitatively, we still have a supercritical Hopf bifurcation and good agreement between both models at small amplitudes
- However, as we go to larger amplitudes, the two results deviate significantly from each other

# Super- and subcritical Hopf bifurcation

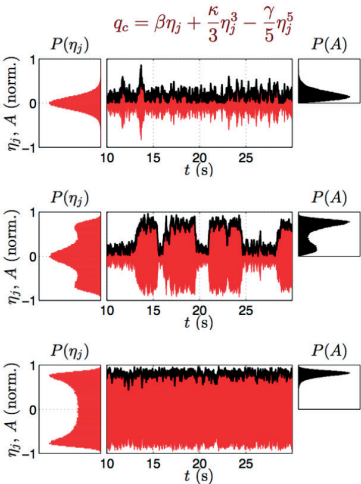
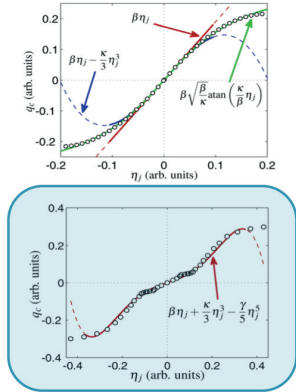


- The three figures on the bottom right show the shape of the potential and the PDF of the acoustic pressure amplitude for different growth rates. We see that for negative  $\nu$  and  $\nu = 0$ , the potential has the same shape as predicted by the Van-der-Pol approach, for large positive  $\nu$ , the potential well is less steep than the cubic nonlinearity would predict at high amplitudes  $A$
- Hence the sigmoid function makes the potential well more smooth. When the system is forced by a stochastic term, this spreads the PDF of the amplitude further to the right



Noiray, JEGTP 2017

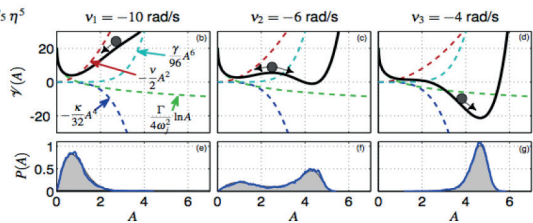
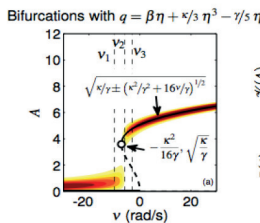
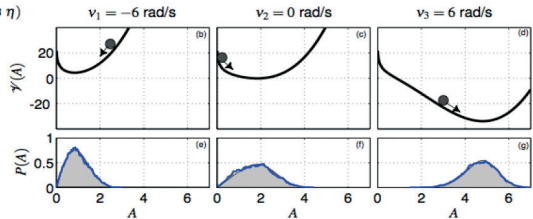
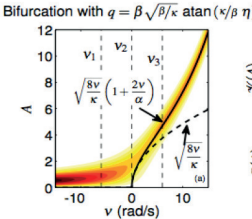
# Super- and subcritical Hopf bifurcation



Noiray, JEGTP 2017

- Now, let's look at the case when we have a flame response with non-monotonous slope as the one shown in the blue box at the bottom left. This seemingly subtle change in the heat release rate function can significantly influence the shape of the amplitude potential, as is shown in the three figures to the right
- On the linearly stable side (top plot), the behavior is basically the same as for the Van-der-Pol oscillator
- However, as  $\nu$  is increased, we have a bistable solution. This is because the damping in our system increases linearly with the modal amplitude  $\eta$ , it is equal to  $\alpha\eta$ ,  $\alpha > 0$ . So if we have a  $q(\eta)$  with monotonous slope, once  $q > \alpha\eta$  at some  $\eta_c$ , then this will be satisfied at all  $\eta > \eta_c$ . However, if we have a  $q(\eta)$  with non-monotonous slope, it can be that  $q$  exceeds the damping at some  $\eta_{c,1}$ , but is smaller than the damping at some higher  $\eta > \eta_{c,2}$ . The end point of such an isolated domain  $[\eta_{c,1}, \eta_{c,2}]$ ,  $\eta_{c,2}$ , represents an attracting point in our potential landscape away from the origin, which lead to the double-peak distribution of the PDF for  $A$  we see in the middle red plot
- Due to the stochastic forcing, we observe in the time series intermittent switches from the low-amplitude attractor at the origin (linearly stable) to the limit cycle and back

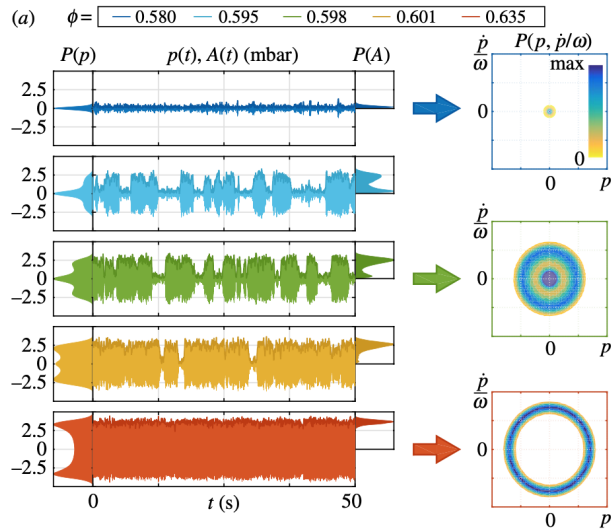
# Super- and subcritical Hopf bifurcation



Noiray, JEGTP 2017

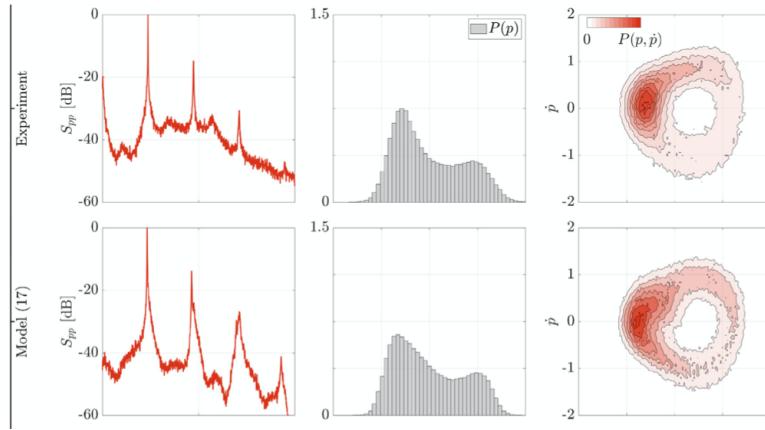
- You can also generate the time traces shown in the last slide with the MATLAB script you received, you just need to modify the nonlinear term. From this, you can obtain the PDFs for  $\eta$ ,  $A$  and also the PSD of the envelope to compute the cut-off frequency
- You can also reconstruct the bifurcation diagram, shown in the bottom left corner, for different growth rates  $v$ . From this diagram, you see that in the linearly stable region, everything is the same as for a linearly stable oscillator
- At high growth rates  $v$  you have a limit cycle with only 1 stable attractor. The main difference is visible near the bifurcation point: This is now a subcritical Hopf bifurcation. The dashed branch is unstable, as we see from the PDF of  $A$
- The three plots on the bottom right show the amplitude potential and the PDF of  $A$ . In the middle plot, the double-well potential, which is underlying the bistable or intermittent behavior we saw in the last slide, is clearly visible. Going back to the bifurcation diagram, we see that this is the region where  $v$  is right between the two stable branches. The stochastic forcing allows for switches back and forth between the two wells

# Super- and subcritical Hopf bifurcation



- Shown to the left is experimental data collected from a turbulent combustor in our lab for a certain burner. For this particular burner, the system exhibits this nonlinear response at a certain frequency
- As we change the equivalence ratio, we go through the bistable regions shown in the figure corresponding to a subcritical Hopf bifurcation. The corresponding dynamics and statistics can be well described by the type of nonlinearity in the oscillator model we just discussed
- Figure from Bonciolini, Ebi, Boujo and Noiray, Royal Society Open Science 2018, <http://dx.doi.org/10.1098/rsos.172078>

# Low-order modelling of nonlinear flame responses with time delays and non-antisymmetric response



- Effect of time delays and quadratic nonlinearities are discussed in Bonciolini, Faure-Beaulieu, Bourquard and Noiray, Combustion and Flame 2021, <https://doi.org/10.1016/j.combustflame.2020.12.034>